Ginsenoside Rh1 inhibits tumor growth in mice with colorectal cancer and depressive symptoms via modulation of the gut microbiota and tumor microenvironment

TINGTING DAI[1,2*], LINGCHANG LI[3*], JIAXIN LI[3], XIAOBIN TAN[3], YI LUO[3], XUEDONG WANG[3], JIE SONG[3], SUJUAN LI[3] and SONGSHAN SHI[1]

[1]Department of Urinary Surgery, Nanjing Integrated Traditional Chinese and Western Medicine Hospital Affiliated with Nanjing University of Chinese Medicine, Nanjing, Jiangsu 210014, P.R. China; [2]Department of Oncology, Nanjing Jinling Hospital, Affiliated Hospital of Medical School, Nanjing University, Nanjing, Jiangsu 210000, P.R. China; [3]Ultrasonic Department, Affiliated Hospital of Integrated Traditional Chinese and Western Medicine, Nanjing University of Chinese Medicine, Nanjing, Jiangsu 210023, P.R. China

Received April 22, 2025; Accepted September 10, 2025

DOI: 10.3892/mmr.2025.13710

Abstract. Depression can accelerate the progression of colorectal cancer (CRC), and depressive remission improves cancer outcomes. Ginsenoside Rh1, the main metabolite of a steroidal saponin extracted from *Panax ginseng*, improves memory and learning and to inhibit tumor growth. However, its anticancer effects and mechanisms in CRC complicated by psychological stress remain unclear. The present study aimed to investigate the protective effect of Rh1 against CRC with coexisting symptoms of depression. A CRC xenograft mouse model exposed to chronic restraint stress (CRS) was established. Behavioral changes, 5-hydroxytryptamine (5-HT) levels, cytokine expression, intestinal microbiota diversity, T-cell recruitment, myeloid-derived suppressor cell (MDSC) proportions and dendritic cell (DC) maturation were analyzed following treatment of the mice with Rh1. Results showed that Rh1 inhibited tumor growth, ameliorated depressive-like behaviors, enhanced cognitive function, upregulated brain 5-HT and serum noradrenaline levels, and decreased serum cortisol, corticotropin-releasing hormone, adrenaline, interleukin-6, C-X-C motif chemokine ligand 1 and tumor necrosis factor-α levels in mice with CRC under CRS. Furthermore, Rh1 intervention attenuated gut dysbiosis and decreased the Firmicutes/Bacteroidota ratio. Antibiotic-induced depletion of gut bacteria further confirmed the involvement of gut microbiota in the anticancer and antidepressant effects of Rh1. Rh1 also promoted T cell activation and DC maturation, and reduced MDSC frequency, thereby reshaping the immune microenvironment. These findings indicate that Rh1 inhibited CRC tumor growth in the CRS-exposed mice by stimulating the immune response and modulating the gut microbiota. Thus, it is suggested that Rh1 has potential as a novel therapeutic strategy for patients with CRC and depression.

Correspondence to: Professor Songshan Shi, Department of Urinary Surgery, Nanjing Integrated Traditional Chinese and Western Medicine Hospital Affiliated with Nanjing University of Chinese Medicine, 179 Xiaolingwei, Xuanwu, Nanjing, Jiangsu 210014, P.R. China
E-mail: shisongshan@sina.com

Professor Sujuan Li, Ultrasonic Department, Affiliated Hospital of Integrated Traditional Chinese and Western Medicine, Nanjing University of Chinese Medicine, 138 Xianlin Avenue, Qixia, Nanjing, Jiangsu 210023, P.R. China
E-mail: lisujuan@jsatcm.com

*Contributed equally

Key words: ginsenoside rh1, colorectal cancer, depression, chronic restraint stress, gut microbiota

Introduction

Among solid tumors, colorectal cancer (CRC) ranks among the most common causes of morbidity and mortality, and its prevalence continues to rise (1). The 5-year survival rate of patients with early-stage localized CRC is >90%, whereas that of patients with metastatic CRC is only 14% (2). There is evidence to suggest that CRC development is influenced by both intrinsic and extrinsic factors. In particular, dysregulated gut microbiota composition has been demonstrated to influence the immune microenvironment and promote distant metastases, and gut microbiota are increasingly recognized as pathogenic contributors to CRC metastasis (3).

Patients with cancer often have a poor prognosis and experience ongoing psychological distress following cancer diagnosis, surgery, chemotherapy and other cancer-related complications (4). Prolonged stress can impair the immune system by changing the metabolic characteristics and composition of the gut microbiota (5), and is a major risk factor that can accelerate CRC development (6). In addition, long-term stress in patients with cancer may reduce their ability to respond to treatments that rely on antitumor immune activity, particularly immunotherapies (7). Therefore, strategies to reduce the effect

of psychological stress and depression on treatment outcomes are crucial.

The association between long-term stress and the growth of tumors is becoming increasingly evident, particularly through neuroimmune interactions (6). Aside from cancer, chronic stress has been shown in numerous studies to stimulate the sympathetic nervous system (8,9), leading to the release of neurotransmitters or hormones that regulate the activity of macrophages, dendritic cells (DCs) and cytotoxic T lymphocytes (10). DCs are immune cells that play a key role in influencing the tumor microenvironment (TME), processing and transmitting antigens, and activating tissue-specific T-cell responses (11). In mice, prolonged psychological stress causes the significant dysregulation of T-cell functions, including reduced cytokine production and impaired cytotoxicity (12), ultimately contributing to metastasis. Disturbances of the microbiota-gut-brain axis and gut microbial balance have been implicated in both depression and CRC pathogenesis. This axis has emerged as a novel target for depression since it mediates communication between the brain and intestinal flora (13).

Traditional Chinese medicine has been widely used to treat CRC, where it may reduce treatment resistance and adverse effects, promote cancer cell death and inhibit metastasis (14). Ginseng, which is widely used in traditional Chinese medicine, contains a variety of active components, including polyacetylenes, ginsenosides and polysaccharides (15). Among these, ginsenosides have been shown to strengthen resistance to stress, boost immunity, and protect the nervous system, with ginsenoside Rh1 (Rh1) having been shown to improve memory and learning by promoting cell viability in the hippocampal region (16). Rh1 is the main metabolite of protopanaxatriol-type ginsenoside Rg1 (17). Rg1 is a natural steroidal saponin extracted from *Panax ginseng* with potent neuroprotective, anti-inflammatory and antidepressant effects (18,19). Notably, Rh1 exhibits stronger effects than its precursor Rg1 in the enhancement of memory and hippocampus excitability (20). These findings suggest that the antidepressive ability of Rh1 is closely associated with the *in vivo* metabolism of Rg1.

Rh1 has demonstrated anti-inflammatory and antitumor properties, mediated by the inhibition of angiogenesis and metastasis (15,21). In particular, Rh1 has been reported to prevent the growth of colon and breast cancers (22,23). However, few studies have investigated the mechanisms by which Rh1 impacts CRC via modulation of the gut microbiota or immune responses, and the impact of Rh1 on CRC under chronic stress conditions remains unclear. In the present study, a CRC mouse model subjected to chronic restraint stress (CRS) was used to explore the antidepressant effect of Rh1, and to evaluate the relationship between Rh1 treatment and the microbial composition of the gut. Furthermore, the study aimed to determine whether the underlying mechanism involves the promotion of DC maturation, thereby activating T cells and enhancing the antitumor immune response to retard CRC progression.

Materials and methods

Cell culture. The Cell Bank of Type Culture Collection of The Chinese Academy of Sciences supplied the CT26 murine colon adenocarcinoma cell line (cat. no. SCSP-523). The cells were cultivated in RPMI-1640 complete medium containing 10% fetal bovine serum (both Jiangsu KeyGEN BioTECH Co., Ltd.), supplemented with 1% penicillin/streptomycin at 37˚C with 5% CO_2.

Animal care. A total of 90 male SPF BALB/c mice (age, ~8 weeks; weight, 20-22 g) were purchased from Shanghai SLAC Laboratory Animal Co., Ltd. The mice were kept in a climate-controlled environment at a temperature of 22±2˚C and a relative humidity of 50±10%, with a 12-h light/dark cycle and free access to food and water. Humane endpoints were established, including >20% weight loss, tumor volume >2,000 mm^3, ulceration, necrosis or infection on the surface of the tumor, abnormal posture or dyspnea. However, no mice were humanely sacrificed or found dead during the study. The maximum weight loss observed was 6.1%. At the end of the experiment, all mice were anesthetized with an intraperitoneal injection of 50 mg/kg pentobarbital sodium. Then, 300 μl blood was collected from the mice by retro-orbital puncture. Afterwards, the mice were sacrificed by cervical dislocation, and death was confirmed by the absence of breathing and heartbeat for >5 min.

Experimental design and drug administration protocols. The CRS model was used to induce depression-like behaviors in mice (24). All mice were randomly assigned to five groups on day 0, following 7 days of adaptation (n=5/group): i) Control group (CRC); ii) model group (CRC + CRS); iii) low dose Rh1 group (CRC + CRS + Rh1 10 mg/kg); iv) high dose Rh1 group (CRC + CRS + Rh1 20 mg/kg); and v) fluoxetine group (CRC + CRS + fluoxetine 10 mg/kg). The doses of Rh1 (Shanghai Yuanye Biotechnology Co., Ltd.) were selected on the basis of a preliminary experiment, in which it was found that 10 and 20 mg/kg Rh1 are able to inhibit both tumor growth and depression. Fluoxetine (Sigma-Aldrich) was employed as a positive antidepressant control. The 10 mg/kg dose of fluoxetine hydrochloride powder was administered by gavage following dilution with distilled water (25). CRS was used to induce depression in the mice prior to tumor implantation. The mice subjected to CRS endured physical restriction for 8 h/day (from 9:00 to 17:00), starting 21 days prior to the start of CT26 cell injection and continued for a total of 42 days (Fig. 1A).

CRS model establishment. All mice except those in the control group were put in a 50-ml conical tube with adequate ventilation to enable easy breathing for 8 h daily, continuously for 42 days in a row, thereby establishing the CRS model. By contrast, the mice in the control group were undisturbed in their cages, without food and water, over the same time periods. After the CRS procedure, the animals were returned to their home cages. At the end of the experiment, on day 42, behavioral assessments were performed, namely the open field test (OFT), the sucrose preference test (SPT) and the elevated plus maze test (EPMT).

CRC tumor model establishment. To establish the CRC model, $1x10^6$ CT26 cells suspended in 0.1 ml PBS were subcutaneously injected into the right flank of each mouse on day 21. The tumors reached ~100 mm^3 in volume 7 days after CT26

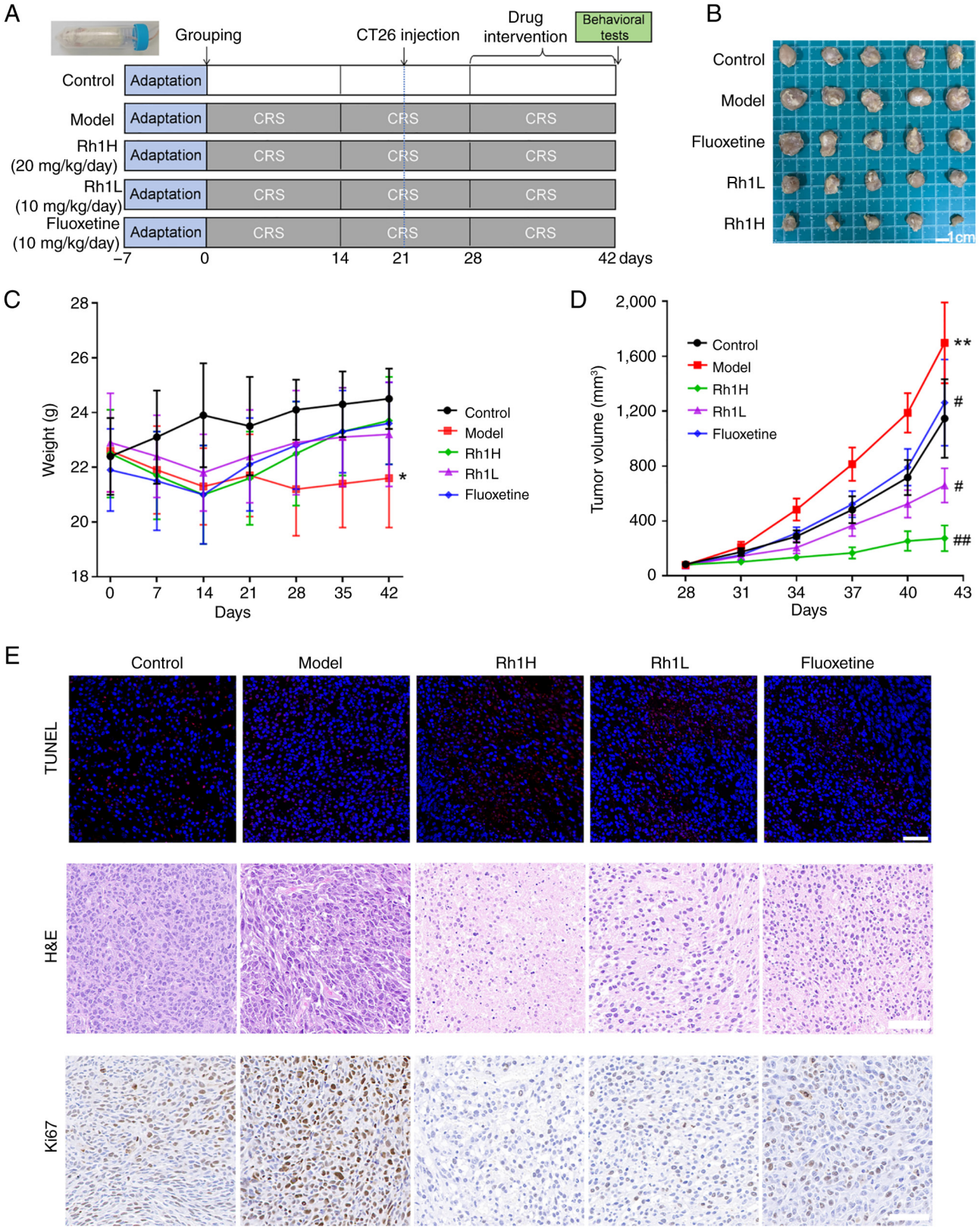

Figure 1. Rh1 treatment inhibits tumor growth in mice with colorectal cancer and CRS. (A) Experimental schedule and treatment groups. (B) Representative images of the excised tumors. (C) Body weights and (D) tumor volume measurements taken during the CRS procedure. Results are presented as the mean ± SD (n=5). *P<0.05 and **P<0.01 vs. the control group; $^{\#}$P<0.05 and $^{\#\#}$P<0.01 vs. the model group. (E) Representative TUNEL, H&E and Ki67 immunohistochemical staining images of the tumors; scale bar, 50 μm. Rh1, ginsenoside Rh1; Rh1H, high dose Rh1; Rh1L, low dose Rh1; CRS, chronic restraint stress; H&E, hematoxylin and eosin.

cell inoculation. The mice were then subjected to treatment with 10 or 20 mg/kg Rh1, or 10 mg/kg fluoxetine. Both Rh1 and fluoxetine were orally administered for 2 weeks, from day 28 to 42. The control and model groups both received the

vehicle orally over the same time period. A caliper was used to measure the volume of the tumor every 3 days, and the tumor volume was calculated using the following formula: $V=(L \times W^2)/2$, where V, L and W represent the volume, length and width of the tumor, respectively. Photographs of the tumors were captured after immersion in formalin.

OFT. The OFT was conducted as described previously (26). Mice were placed in a 50x50x50-cm open-field arena with a black floor and blue Plexiglas walls. Each mouse was allowed to spontaneously explore the arena for 5 min. Following each trial, 75% ethanol was used to clean the apparatus to remove odors. The following parameters were measured: Total distance traveled, distance traveled in the central area and dwelling time in the central area (27).

EPMT. The EPMT was performed as previously described, with refinements (28). The plus-maze apparatus consisted of four arms arranged in a cross, elevated 90 cm above the floor. Two of the arms were closed and two were open. Mice were placed on the central platform facing an open arm and allowed to explore the apparatus for 5 min. During this period, the behavior of the mice was recorded, and the time spent and distance traveled in the open arms was examined.

SPT. The SPT was conducted as previously described (29). Mice were individually housed in a cage containing two bottles of 1% sucrose solution for 24 h. This was followed by 24 h of food and water deprivation. After adaption, the mice were given free access to two identical bottles, one containing a 1% sucrose solution and the other containing water. The volumes of water and sucrose solution consumed were measured, and the percentage of sucrose solution to total fluid consumed was calculated to indicate sucrose preference.

Antibiotics (ABX) treatment. Pseudo germ-free BALB/c mice were established by the administration of ABX solution to depleting the endogenous gut microbiota and to investigate the causal role of gut microbiota. The ABX solution contained neomycin (1 g/l), ampicillin (1 g/l), metronidazole (1 g/l) and vancomycin (500 mg/l) in autoclaved water (30). This combination was selected for its broad-spectrum activity (covering Gram-positive and -negative bacteria, and anaerobes) to ensure maximal depletion of gut microbial communities. The ABX solution was orally administered to the mice for consecutive 21 days starting on day 21, with replacement of the drinking water every 2 days. The ABX treatment was designed to establish a causal link between gut microbiota and the Rh1 treatment response and to explore whether the effect of Rh1 was microbiota-dependent.

Assessments of inflammatory factors and hormones. The blood collected by retro-orbital puncture was centrifuged 3,500 x g for 12 min at 4˚C to isolate the serum. In addition, mouse brains were collected, homogenized in saline on ice, and the homogenates were centrifuged 6,000 x g for 15 min at 4˚C. The supernatant was carefully transferred to a sterile tube and stored at -20˚ until required for analysis. Noradrenaline (NE), adrenaline, cortisol (CORT), corticotropin-releasing hormone (CRH), interleukin-6 (IL-6), tumor necrosis factor-α (TNF-α) and C-X-C motif chemokine ligand 1 (CXCL1) in the serum and 5-hydroxytryptamine (5-HT) in the brain were measured using the following ELISA kits: NE (cat. no. E-EL-0047; Wuhan Elabscience Biotechnology Co., Ltd.), adrenaline (cat. no. E-EL-0045; Wuhan Elabscience Biotechnology Co., Ltd.), CORT (cat. no. AD3213Mo; Andy Gene Biotechnology Co., Ltd.), CRH (cat. no. E-EL-M0351; Wuhan Elabscience Biotechnology Co., Ltd.), IL-6 (cat. no. PI326; Beyotime Institute of Biotechnology), TNF-α (cat. no. PT512; Beyotime Institute of Biotechnology), CXCL1 (cat. no. PC173; Beyotime Institute of Biotechnology) and 5-HT (cat. no. E-EL-0033; Wuhan Elabscience Biotechnology Co., Ltd.).

Histopathological analysis and immunohistochemical staining. Tumors were excised from the animals and immediately fixed in 4% paraformaldehyde at room temperature for 48 h. For hematoxylin and eosin (H&E) staining, deparaffinized and rehydrated 4-μm-thick sections were stained with hematoxylin solution at room temperature for 5 min. Sections were stained with 0.5% eosin Y solution at room temperature for 3 min. After staining, sections were dehydrated, cleared in xylene, and mounted with neutral balsam. Immunohistochemical staining was also performed. The 4-μm-thick tumor sections were blocked with 3% BSA (Sigma-Aldrich) for 30 min at 37˚C, subjected to peroxidase quenching with 3% hydrogen peroxide for 10 min at room temperature and then incubated with an anti-Ki67 primary antibody (cat. no. ab15580; Abcam, 1:500) overnight at 4˚C. Subsequently, the sections were incubated with HRP-labeled secondary antibody (cat. no. ab6721; Abcam, 1:1,000 dilution) for 1 h at 37˚C, and then counterstained with hematoxylin (5 min at room temperature). Both H&E and Ki67 staining were observed under a bright-field light microscope (Olympus BX53).

TUNEL assays. Paraffin sections (3 μm thick) were prepared from the tumors. An *In Situ* Cell Death Detection Kit (cat. no. 11684817910; Roche Diagnostics GmbH) was used to detect apoptotic cells in the sections. A total of 50 μl TUNEL reaction mixture was added at 37˚C for 45 min. After incubation, sections were washed with PBS. Nuclei were counterstained with DAPI (cat. no. ab104139; Abcam) at a concentration of 2 μg/ml at room temperature for 8 min, while red fluorescence indicated the apoptotic nuclei. Tissue sections were visualized under a fluorescence microscope (Zeiss Axio Imager Z2, Carl Zeiss AG). For quantification, four random fields were chosen from each section and the average percentage of positive cells in each field was calculated.

Immunofluorescence staining. 3 μm-thick tumor sections were subjected to deparaffinization and rehydration. Sections were immersed in 0.01 M sodium citrate buffer, and heated in a microwave. Endogenous peroxidase activity was quenched with 3% hydrogen peroxide for 10 min at room temperature. Sections were then covered with 5% goat serum (cat. no. GB25004; Wuhan Servicebio Technology Co., Ltd.) to block non-specific binding at room temperature for 30 min. For CD11c/CD80 dual staining, tumor sections were first incubated with anti-CD11c antibody (cat. no. ab254183; Abcam, 1:200) at 4˚C overnight, followed by anti-mouse IgG H&L

(HRP) (cat. no. GB23301; Wuhan Servicebio Technology Co., Ltd., 1:500 dilution) at room temperature for 1 h. Cyanine 3 tyramide (cat. no. G1233; Servicebio, 1:50 dilution) was then incubated at room temperature for 10 min to amplify the HRP signals, producing red fluorescence. Sections were subsequently incubated with FITC-conjugated anti-CD80 antibody (cat. no. ZB115640; Wuhan Servicebio Technology Co., Ltd., 1:100 dilution) at room temperature for 1 h, which generated green fluorescence. For CD8 staining, sections were incubated with anti-CD8 antibody (cat. no. GB115692; Wuhan Servicebio Technology Co., Ltd., 1:200 dilution) at 4˚C overnight, followed by FITC-conjugated IgG (H+L) secondary antibody (cat. no. GB22303; Wuhan Servicebio Technology Co., Ltd., 1:500) at room temperature for 1 h. After staining, all sections were counterstained with DAPI (working concentration: 2 μg/ml, cat. no. ab104139; Abcam) at room temperature for 8 min. The stained sections were observed using a fluorescence microscope (Zeiss Axio Imager Z2, Carl Zeiss AG).

16S rRNA sequencing and data analysis. Mice fecal samples were collected on day 42, at the end of the experiment, and were snap frozen in liquid nitrogen and stored at -80˚C until use. Total DNA was extracted from the fecal samples using the FastPure Feces DNA Isolation Kit (Shanghai Major Yuhua Co., Ltd.) according to the manufacturer's instructions. DNA concentration and purity were assessed using a NanoDrop2000 spectrophotometer (Themo Fisher Scientific, Inc.). The V3-V4 variable region of the 16S rRNA gene was amplified using PrimeSTAR Max DNA Polymerase (cat. no. R045A; Takara Bio Inc., Shiga, Japan),with the universal bacterial primer pair: Forward primer (338F): 5'-ACTCCTACGGGA GGCAGCAG-3'; Reverse primer (806R): 5'-GGACTACHV GGGTWTCTAAT-3'. The thermocycling condition was set as follows: Pre-denaturation: 98˚C for 3 min; Denaturation: 98˚C for 10 sec, 55˚C for 30 sec; Extension: 72˚C for 45 sec; Steps 2-4 repeated for 30 cycles; Final extension: 72˚C for 5 min. Amplicon visualization was verified by 2% agarose gel electrophoresis stained with 0.5 μg/ml ethidium bromide (cat. no. E1510; Sigma-Aldrich, St. Louis, MO, USA). Amplified products were purified using the AMPure XP Beads (cat. no. A63881; Beckman Coulter, Inc., Brea, CA, USA). Then, the Nextera XT DNA Library Prep Kit (cat. no. FC-131-1096; Illumina, Inc., San Diego, CA, USA) was used to construct sequencing libraries. Sequencing was then performed using the MiSeq PE250 system (Illumina, Inc.) with 250 bp paired-end (PE250) sequencing. The MiSeq Reagent Kit v3 (600 cycles, cat. no. MS-102-3003; Illumina, Inc.) was used. After library quality control, qualified libraries were pooled and diluted to a loading concentration of 6 pM. Raw sequencing reads were quality-controlled using FastQC (Version 0.11.9; Babraham Bioinformatics, Cambridge, UK). Paired-end reads were merged into full-length sequences using FLASH (Version 1.2.11). Amplicon sequence variations were generated using Deblur-denoised sequences (Version 1.1.0; github.com/biocore/deblur. The Simpson (measuring community evenness), abundance-based coverage estimator (ACE, estimating species richness) and Shannon (combining richness and evenness) indices (31-33) were determined to evaluate α diversity of the data and principal coordinate analysis (PCoA) was performed to evaluate the b diversity of the data. PCoA visualization was performed using the q2-emperor plugin in QIIME 2 (qiime2.org).

Flow cytometry analysis. The spleen and tumor-draining lymph nodes were each mechanically filtered using a 200-mesh screen. Red blood cells in the resulting cell suspensions were lysed using ACK lysis buffer (cat. no. C3702; Beyotime Institute of Biotechnology). Tumor tissues were mechanically minced and digested in RPMI-1640 medium containing DNase, collagenase IV and hyaluronidase (Gibco; Thermo Fisher Scientific, Inc.) at 37˚C for 1 h. The tissues were filtered through a sieve to prepare a single-cell suspension. Isolated cells were plated and cultured for 4 h in a medium containing Cell Activation Cocktail (cat. no. 423303; BioLegend, Inc.) to analyze the release of cytokines by tumor-infiltrating T cells. Cells were then aliquoted into tubes and surface stained in the dark for 30 min at 4˚C with Fixable Viability Dye eFluor 780 (cat. no. 2633409; eBioscience; Thermo Fisher Scientific, Inc.), anti-CD3-PE-cy7 (cat. no. 552774; BD Biosciences), anti-CD4-APC (cat. no. 100412; BioLegend, Inc.), anti-CD45-Percy-cy5 (cat. no. 103131; BioLegend, Inc.) and anti-CD8-FITC (cat. no. 100706; BioLegend, Inc.). The anti-CD45 antibody is used to gate the 'leukocyte population', and the anti-CD3 antibody is used to identify T cells from the $CD45^+$ leukocyte population. For intracellular staining, cells were fixed with fixation buffer (4% paraformaldehyde, cat. no. 420801; BioLegend, Inc.) in the dark for 30 min at room temperature and washed with permeabilization buffer (cat. no. 421002; BioLegend, Inc.) twice. Cells were incubated with anti-granzyme B-BV421 (cat. no. 396413; BioLegend, Inc.) and anti-IFN-γ-PE (cat. no. 505807; BioLegend, Inc.) in the dark for 30 min at 4˚C.

After blocking with anti-mouse CD16/32 (Fc block, cat. no. 553141, BD Pharmingen), MDSC was examined by staining with Fixable Viability Dye eFluo 780 (eBioscience), anti-CD45-Percy-cy5 (cat. no. 103131; BioLegend, Inc.), anti-CD11b-FITC (cat. no. 101206; BioLegend, Inc.) and anti-Gr-1-APC (cat. no. 108411; BioLegend, Inc.) in the dark for 30 min at 4˚C. After blocking with anti-mouse CD16/32, M-MDSCs was examined by staining with Fixable Viability Dye eFluo 780 (eBioscience), anti-CD45-Alexa Fluor700 (cat. no. 103127; BioLegend, Inc.), anti-CD11b-FITC (cat. no. 101206; BioLegend, Inc.), anti-Ly-6C-PerCP cy5.5 (cat. no. 128011; BioLegend, Inc.) and anti-Ly-6G-PE (cat. no. 127607; all BioLegend, Inc.) in the dark for 30 min at 4˚C. After blocking with anti-mouse CD16/32, DC maturation was examined by staining with Fixable Viability Dye eFluo 780 (eBioscience, USA), anti-CD45-Percy-cy5, anti-CD11c-APC (cat. no. 117309; BioLegend, Inc.), and anti-MHCII-FITC (cat. no. 107605; BioLegend, Inc.) antibodies, or an isotype IgG control (cat. no. 400605; BioLegend, Inc.) in the dark for 30 min at 4˚C. Flow cytometry analysis was performed using an Beckman CytoFLEX flow cytometer (Beckman Coulter Inc.). The flow cytometry data were analyzed using FlowJo software V10.8.1 (BD Biosciences).

Statistical analysis. Data are presented as the mean ± standard deviation for normally distributed data. Non-normally distributed data are presented as the median and 25th and 75th percentile). Statistical analyses were performed using

GraphPad Prism 9.0 software (Dotmatics). When the data displayed a normal distribution and homogeneous variance, one-way ANOVA was employed, followed by Bonferroni post-hoc multiple comparisons tests. When the data displayed a normal distribution and heterogeneous variance, Welch ANOVA was used; no post-hoc test was performed as the results were not statistically significant. When the data were non-normally distributed, Kruskal-Wallis H test was applied, followed by post-hoc pairwise comparisons using Bonferroni-corrected Mann-Whitney U tests. $P<0.05$ was considered to indicate a statistically significant difference.

Results

Rh1 inhibits tumor growth in mice with CRC and CRS. The experimental plan is displayed in Fig. 1A. CRS was applied to induce depression in all mice, with the exception of those in the control group. A CT26 cell-bearing tumor model was established after 3 weeks of CRS. The mean body weight of the mice in the model group at the end of the study was significantly less than that of mice in the control group. Although mean body weight exhibited an ascending tendency in the Rh1 and fluoxetine treatment groups compared with that in the model group, the difference between these groups was not found to be statistically significant (Fig. 1C). Tumor growth in the model group was greater than that in the control group (Fig. 1B). By day 42, the tumor volume in the stressed mice of the model group was significantly higher than that in the non-stressed mice of the control group, but significantly lower in the two Rh1 groups compared with the model group (Fig. 1D).

H&E staining revealed that the tumor cells in the model group were densely packed, exhibiting irregular morphologies, nuclear dimorphism and mitotic figures. In the Rh1 and fluoxetine groups, features of cell necrosis and apoptosis were observed. Necrosis was indicated by dispersed lower-density cells, cytoplasmic leakage, cellular rupture and multiple vacuolar structures, while apoptosis was characterized by nuclear condensation, fragmentation and dissolution (Fig. 1E). In addition, the number of TUNEL positive cells in the Rh1 groups was increased markedly compared with that in the model group (Fig. 1E). Furthermore, Rh1 treatment clearly reduced Ki67 expression in tumors to lower levels than those observed in the model group. These findings indicate that Rh1 attenuates tumor development in mice with CRC and CRS.

Rh1 ameliorates depressive-like behaviors and enhances cognitive function in mice with CRC and CRS. The therapeutic impact of low and high dosages of Rh1 was assessed using the stress-associated cancer model mice (Fig. 2). Depression- and anxiety-like behaviors were evaluated using the SPT, EPMT and OFT. In the OFT, the depressed mice in the model group exhibited a reduced capacity for spontaneous exploration and tended to remain in the corners and edges of the field (Fig. 2A). The total distance traveled, distance traveled in the central area and dwelling time in the central area of the model mice were significantly decreased compared with those of the control group (Fig. 2B). However, these measures were significantly increased in the mice treated with fluoxetine or Rh1 compared with those in the model group.

The results of the EPMT assay revealed that the time spent and distance traveled in the open arms by the model mice were significantly lower compared with those of the control mice (Fig. 2C and D). However, following Rh1 or fluoxetine intervention, significant increases in the time spent and distance traveled in the open arms were observed.

The SPT is regarded as an index of anhedonia. Sucrose preference decreased significantly in model group compared with that in the control group. However, the Rh1H and fluoxetine groups exhibited significantly increase sucrose preference rates compared with that of the model group (Fig. 2E). These results indicate that Rh1 treatment attenuated the abnormal behaviors of CRS rats in the SPT, EPMT and OFT, and suggest that both fluoxetine and Rh1 alleviate depression-like behaviors in mice.

Rh1 regulates cytokine expression and hormone levels in mice with CRC and CRS. Cytokines are essential contributors to the regulation of inflammatory processes. ELISA results revealed that the levels of TNF-α, IL-6 and CXCL1 were significantly higher in CRS-exposed mice with CRC compared with those in control mice with CRC, indicating that CRS increased the inflammatory response in mice with CT26 tumors (Fig. 3A). The levels of TNF-α, CXCL1 and IL-6 in the Rh1 and fluoxetine groups were considerably lower compared with those in the model group. Reductions in the levels of the monoamine neurotransmitters 5-HT and NE, and increases in CORT levels are associated with depression (34). In particular, alterations in the release or reuptake of 5-HT are associated with depressive disorder. Mice in the CRS-stimulated CRC-bearing model group exhibited significantly lower brain 5-HT and serum NE levels compared with those in the control group, indicating that CRS stimulation disrupts monoamine neurotransmitter homeostasis. Treatment with Rh1 or fluoxetine resulted in significant increases in these levels (Fig. 3). Adrenaline is a key catecholamine hormone released during stress and may influence cancer progression (35). The serum levels of adrenaline, CRH and CORT in the model group were significantly higher compared with those in the control group; however, treatment with a high dose of Rh1 or fluoxetine resulted in a significant reduction in these levels (Fig. 3B).

Rh1 rebalances gut dysbiosis in mice with CRC and CRS. The results of α-diversity analyses indicated that the gut microbial communities in all five groups were rich and diverse. In the model group, the Simpson index was significantly higher and the ACE and Shannon indices were significantly lower compared with those in the control group. ACE indices in the Rh1 or fluoxetine groups were not significantly different from that of the model group. The Simpson indices of the Rh1 and fluoxetine groups were significantly lower than that of the model group. The Shannon indices of the Rh1 and fluoxetine groups were significantly higher than the Shannon index of the model group (Fig. 4A). Furthermore, b diversity was analyzed using PCoA based on various distance measures, including Bray-Curtis distances. When plotted against the relative contributions of each group to each principal component (PC), the first two principal components, which together

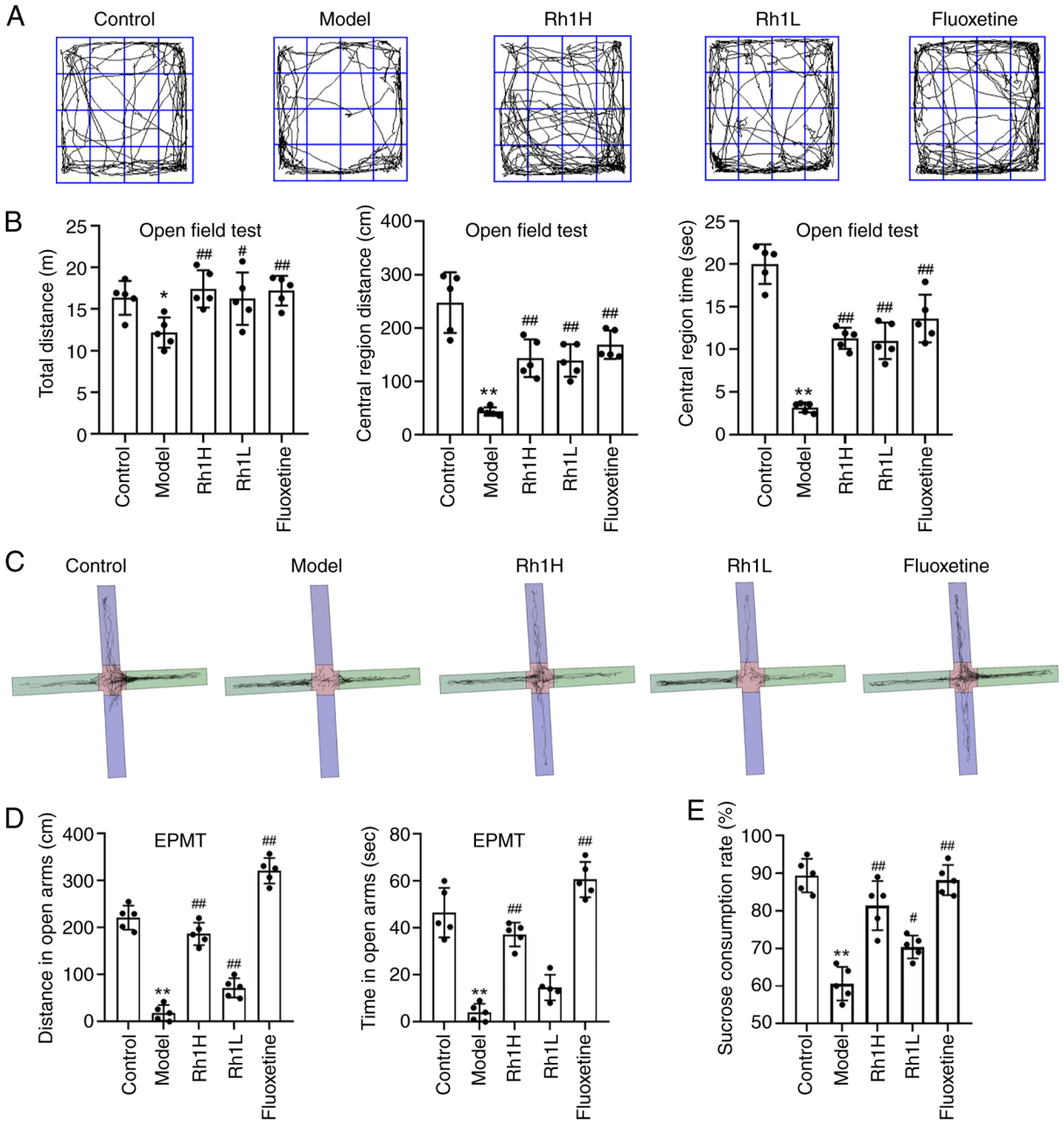

Figure 2. Rh1 treatment alleviates depression-like behaviors in mice bearing colorectal tumors and subjected to chronic restraint stress. (A) Representative trajectory plots from the OFT. (B) Total distance traveled, distance traveled in the central region and time spent in the central region during the OFT. (C) Representative trajectory plots from the EPMT. (D) Total distance traveled and time spent in the open arms during the EPMT. (E) Sucrose consumption data from the sucrose preference test. Results are presented as the mean ± SD (n=5). *P<0.05 and **P<0.01 vs. the control group; $^{\#}$P<0.05 and $^{\#\#}$P<0.01 vs. the model group. Rh1, ginsenoside Rh1; Rh1H, high dose Rh1; Rh1L, low dose Rh1; OFT, open field test; EPMT, elevated plus maze test.

accounted for 39.80% of the total microbial factor loadings (PC1, 22.76%; PC2, 17.04%), revealed notable differences in the gut microbiota communities among the groups. In the Rh1-treated groups, clear shifts in bacterial composition towards that of the control group were observed (Fig. 4B), indicating partial restoration of the gut microbial community. Proteobacteria, Firmicutes, Bacteriodota, Actinobacteriota and Desulfobacterota accounted for the majority of the sequencing reads among the phyla that were detected (Fig. 4C). When compared with the microbial composition of the control group, the model group exhibited a significantly higher abundance of Firmicutes and Actinobacteriota, lower abundance of Bacteroidota and Proteobacteria (Fig. 4D), and a higher Firmicutes/Bacteroidota ratio (Fig. 4E). Exposure to a high dose of Rh1 significantly increased the abundance of Bacteroidota and reduced the abundance of Firmicutes. Mice treated with a low dose of Rh1 also exhibited a significantly reduced abundance of Firmicutes.

A Spearman correlation heatmap revealed that Bacteroidota abundance positively correlated with 5-HT and NE (Fig. 4F), and negatively correlated with TNF-α, CXCL1, adrenaline and CRH. It also revealed that Firmicutes abundance negatively correlated with 5-HT and NE, and positively correlated with TNF-α, CXCL1 and CRH. In addition, the inflammatory factor IL-6 and Proteobacteria exhibited a

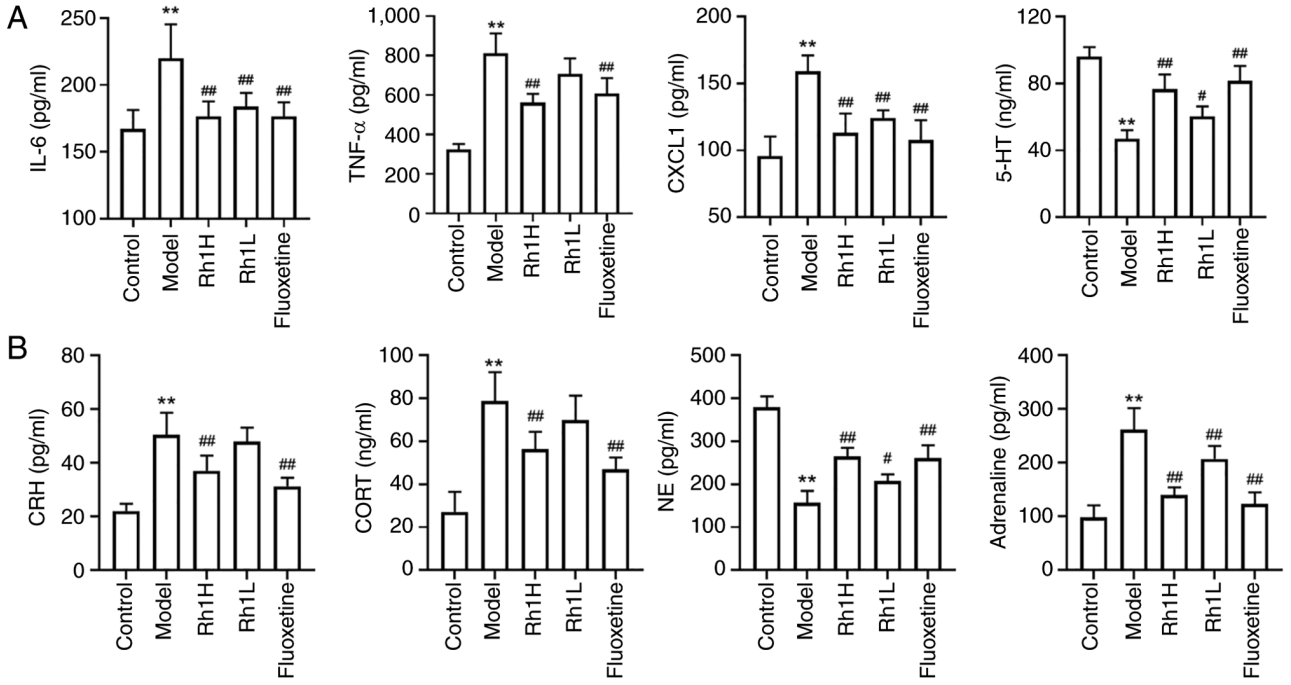

Figure 3. Rh1 regulates the levels of hormones and inflammatory factors in the brain and serum of mice bearing colorectal tumors and subjected to chronic restraint stress. (A) Brain levels of 5-HT and serum levels of TNF-α, IL-6 and CXCL1. (B) Serum levels of adrenaline, NE, CRH and CORT. Results are presented as the mean ± SD (n=5). **P<0.01 vs. the control group; $^{\#}$P<0.05 and $^{\#\#}$P<0.01 vs. the model group. Rh1, ginsenoside Rh1; Rh1H, high dose Rh1; Rh1L, low dose Rh1; IL-6, interleukin-6; TNF-α, tumor necrosis factor-α; CXCL1, C-X-C motif chemokine ligand 1; 5-HT, 5-hydroxytryptamine; CRH, corticotropin-releasing hormone; CORT, cortisol; NE, noradrenaline.

negative correlation, while the endocrine hormone CORT and Desulfobacterota exhibited a positive correlation.

Gut microbiota mediates the antitumor effect of Rh1 in mice with CRC and CRS. We hypothesized that the efficacy of Rh1 in treating cancer comorbid with depression may be mediated by gut bacteria, given the importance of intestinal flora in both carcinogenesis and depression (36). ABX treatment was administered to decrease the resident microbiota in mice subjected to CRS during Rh1 intervention (Fig. 5A). The amelioration of depression-like behaviors observed in the OFT for the high dose Rh1 group was attenuated when the mice also received ABX treatment (Fig. 5C). No significant differences were observed between the mice in the model group and those treated with both ABX and high dose Rh1 with regard to the total distance traveled and the distance traveled in the central area. The time in the central region in ABX + Rh1H group were considerably lower than that of Rh1H group. The antitumor effect of Rh1 in mice with CRS and CRC may be weakened by the reduction of gut flora, as suggested by the significantly larger mean tumor volume in the mice treated with ABX and high dose Rh1 compared with that in mice treated with high dose Rh1 alone (Fig. 5B).

Rh1 improves T-cell activation in mice with CRC and CRS. The effect of Rh1 on immune cell infiltration and activation in mice with CRC and CRS was investigated (Fig. 6). Examination of $CD8^+$T and $CD4^+$T cell subsets in the tumors revealed that mice in the high dose Rh1 group had a significantly higher population of effector T cells (IFN-γ^+CD8^+T cells and IFN-γ^+CD4^+T cells) compared with that in the model group (Fig. 6A). These data indicate that increased activation of $CD8^+$ and $CD4^+$ T cells increases IFN-γ production in tumor tissues, which may serve as a key mediator of the tumor rejection response. In addition, by significantly increasing the percentage of granzyme B^+ cells within the $CD8^+$T and $CD4^+$T cell population, Rh1 may restore the functional activity of tumor-infiltrating $CD8^+$T and $CD4^+$T cells (Fig. 6B). Furthermore, immunofluorescence staining indicated that CD8-positive T cells exhibited weaker red fluorescence in the model group compared with that in the control group, while CD8-positive T cells were markedly increased in the high dose Rh1 group (Fig. 6C).

The spleens of mice treated with a high dose of Rh1 had a significantly higher frequency of IFN-γ^+CD4^+T cells than that observed in the model group (Fig. 7A). Treatment with a high dose of Rh1 also raised the proportion of $CD8^+$T cells co-expressing IFN-γ; however, this increase was not statistically significant. Myeloid-derived suppressor cells (MDSCs) isolated from the spleen were also analyzed by flow cytometry. The number of tumor-infiltrating $CD11b^+Gr\text{-}1^+$ cells, considered to represent MDSCs, was analyzed. As shown in Fig. 7B, Rh1 significantly decreased the proportion of total MDSCs in the spleen compared with that in the model group (Fig. 7B). Additionally, the percentages of different MDSC subtypes were evaluated, and the results revealed that after treatment with a high dose of Rh1, the frequency of monocytic MDSCs (M-MDSC, $CD11b^+Ly6G^-Ly6C^{high}$) cells was significantly reduced (Fig. 7C). These findings suggest that $CD8^+$T, $CD4^+$T and MDSC cells may contribute to the antitumor response of Rh1, with Rh1 reducing MDSC counts and promoting the recovery of T cell-dependent antitumor responses.

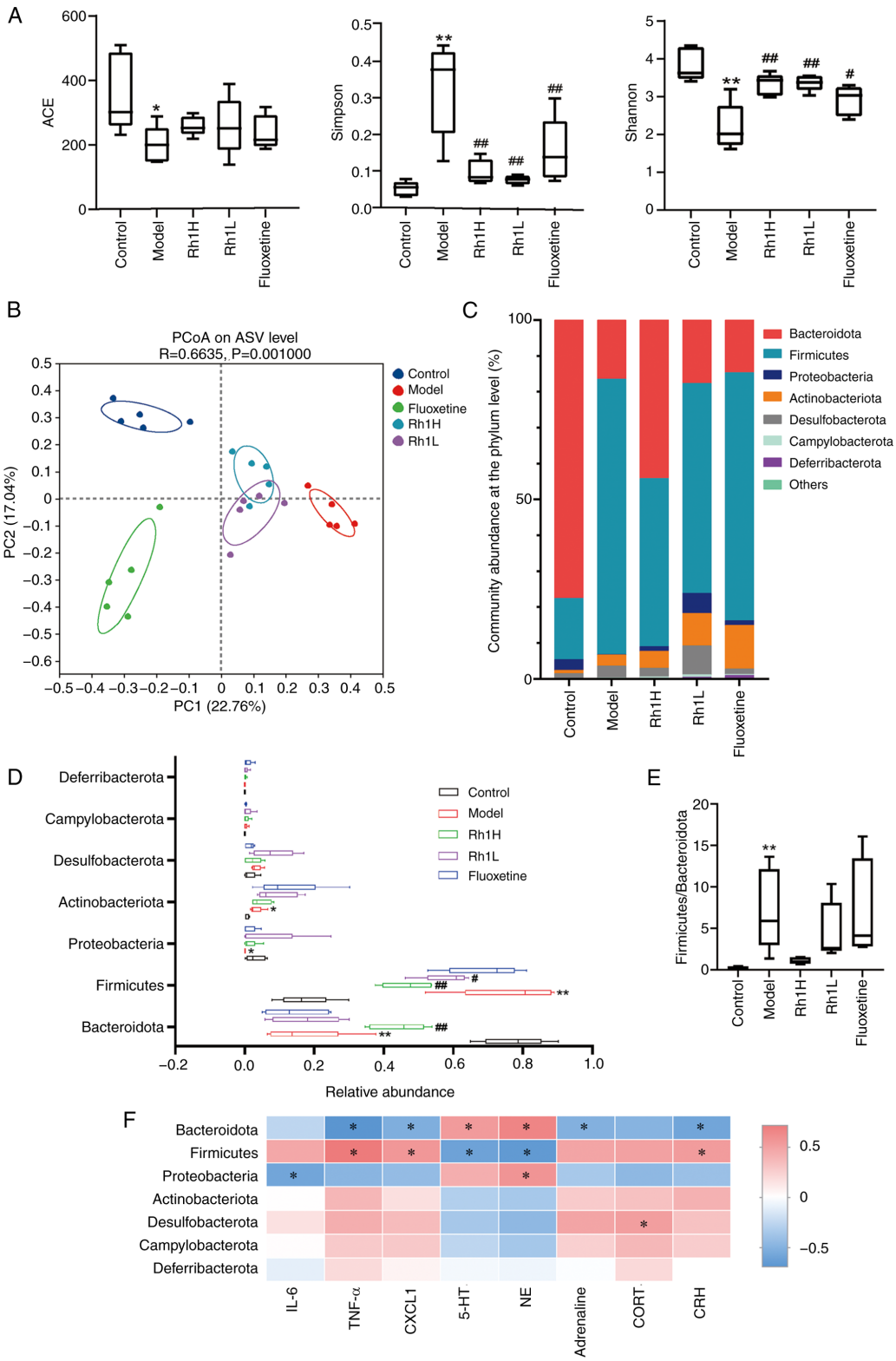

Figure 4. Rh1 treatment regulates the gut microbial balance in mice bearing colorectal tumors and subjected to chronic restraint stress. (A) ACE, Simpson and Shannon indices of α-diversity and (B) PCoA analysis of the β-diversity of the gut microbiota. (C) Community distribution and (D) richness of the intestinal flora at the phylum level. (E) Firmicutes/Bacteroidota ratios. (F) Heat map showing the Spearman correlation coefficients for hormone or inflammatory factors with phylum abundance. n=5). *P<0.05 and **P<0.01 vs. the control group; $^{\#}$P<0.05 and $^{\#\#}$P<0.01 vs. the model group. Rh1, ginsenoside Rh1; Rh1H, high dose Rh1; Rh1L, low dose Rh1; ACE, abundance-based coverage estimator; PCoA, principal coordinate analysis; PC, principal component; ASV, amplicon sequence variant; IL-6, interleukin-6; TNF-α, tumor necrosis factor-α; CXCL1, C-X-C motif chemokine ligand 1; 5-HT, 5-hydroxytryptamine; NE, noradrenaline; CORT, cortisol; CRH, corticotropin-releasing hormone.

Rh1 promotes DC maturation in mice with CRC and CRS. Naive or memory $CD8^{+}$ and $CD4^{+}$T cells are exposed to antigens by mature DCs through MHCI and MHCII molecules, respectively (37). To verify whether DCs

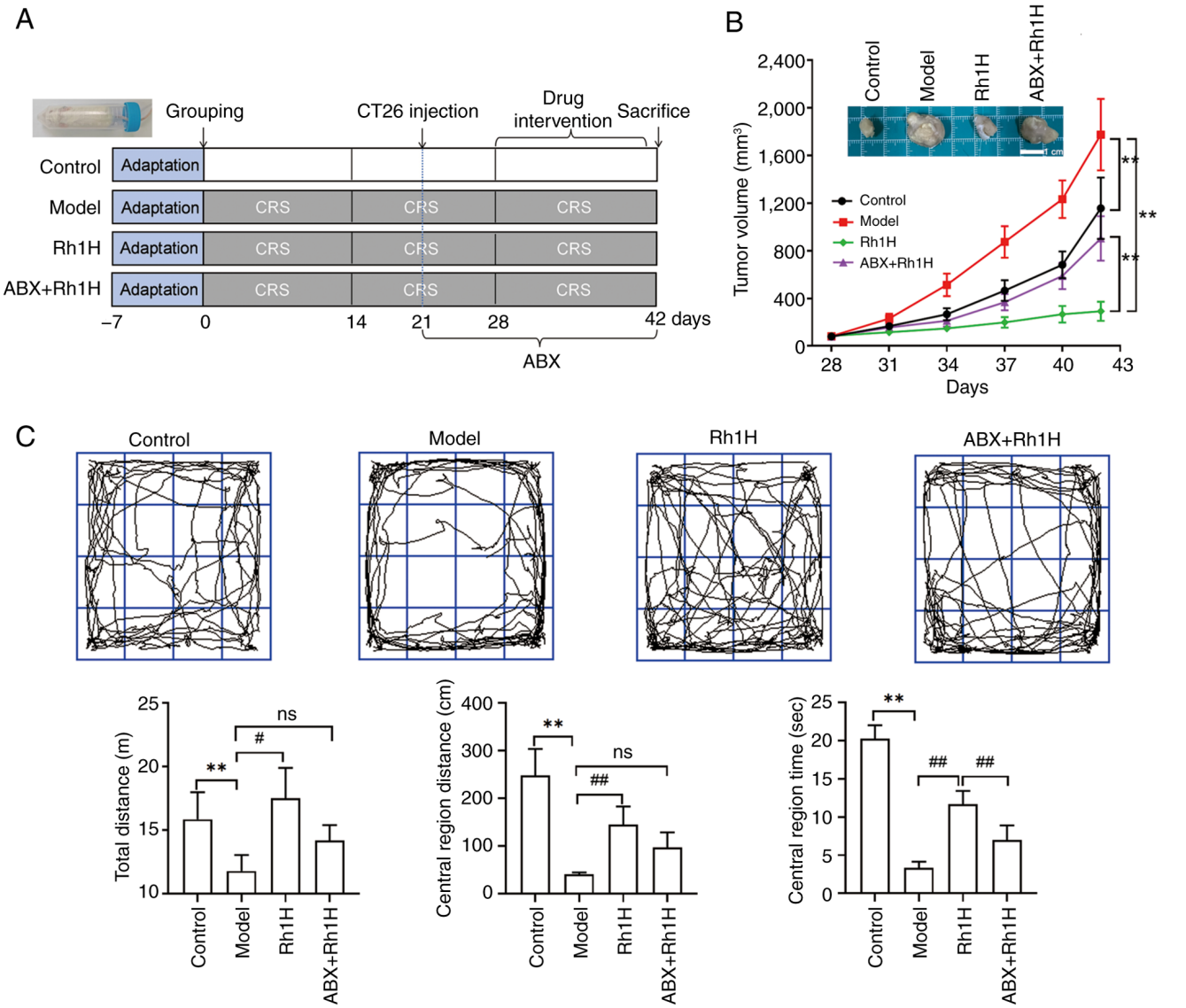

Figure 5. Gut microbiota is involved in the anticancer and antidepressive effect of Rh1. (A) Experimental design for microbiota depletion by ABX in CRS-exposed mice bearing colorectal tumors during Rh1 intervention. (B) Representative images of the tumors, and tumor volume measurements during the CRS procedure. (C) Trajectory plots from the open field test. Results are presented as the mean ± SD (n=5). **P<0.01, $^{\#}$P<0.05 and $^{\#\#}$P<0.01 as indicated. Rh1, ginsenoside Rh1; Rh1H, high dose Rh1; ABX, antibiotics; CRS, chronic restraint stress; ns, not significant.

contributed to the immune response, the maturation of DCs was detected in Rh1-treated CRC tissues, tumor-draining lymph nodes and the spleen. Flow cytometric analysis confirmed that the expression of MHCII, a DC maturation marker, was significantly increased in the spleen, lymph node and tumor tissue following Rh1 treatment compared with that in the model group (Fig. 8A), suggesting the robust accumulation and maturation of DCs in the TME following Rh1 treatment. In addition, immunofluorescence staining indicated that CD80-positive DCs exhibited only weak green fluorescence in the model group (Fig. 8B), but markedly higher green fluorescence in the high dose Rh1 group. These results demonstrate that Rh1 effectively stimulates DCs to cross-present antigens, which in turn activate $CD8^{+}$T cells to enhance the immune response. In addition, Rh1 may have markedly boosted the antitumor immune response by increasing the capacity of activated T cells to eradicate tumor cells.

Discussion

Depression is a prevalent psychological disorder that is a threat to mental well-being worldwide and has resulted in a growing suicide rate during the 21st century (38). CRC is the second most common cause of cancer-related deaths (39). Depression and chronic psychological stress negatively impact the quality of life of patients with CRC. In addition, an increased risk of depression has been observed in patients with CRC following prognosis (40). Therefore, the effective management of comorbid depression has attracted considerable attention.

The Rg1 metabolite Rh1 has demonstrated strong inhibitory effects on the proliferation of lung and breast cancer cells (41), and has been reported to suppress the invasion of CRC and breast cancer cells (22). Research on Rh1 has focused on its anticancer, anti-inflammatory and immune modulating properties (11,42). However, its potential antidepressant effects and the underlying mechanisms remain

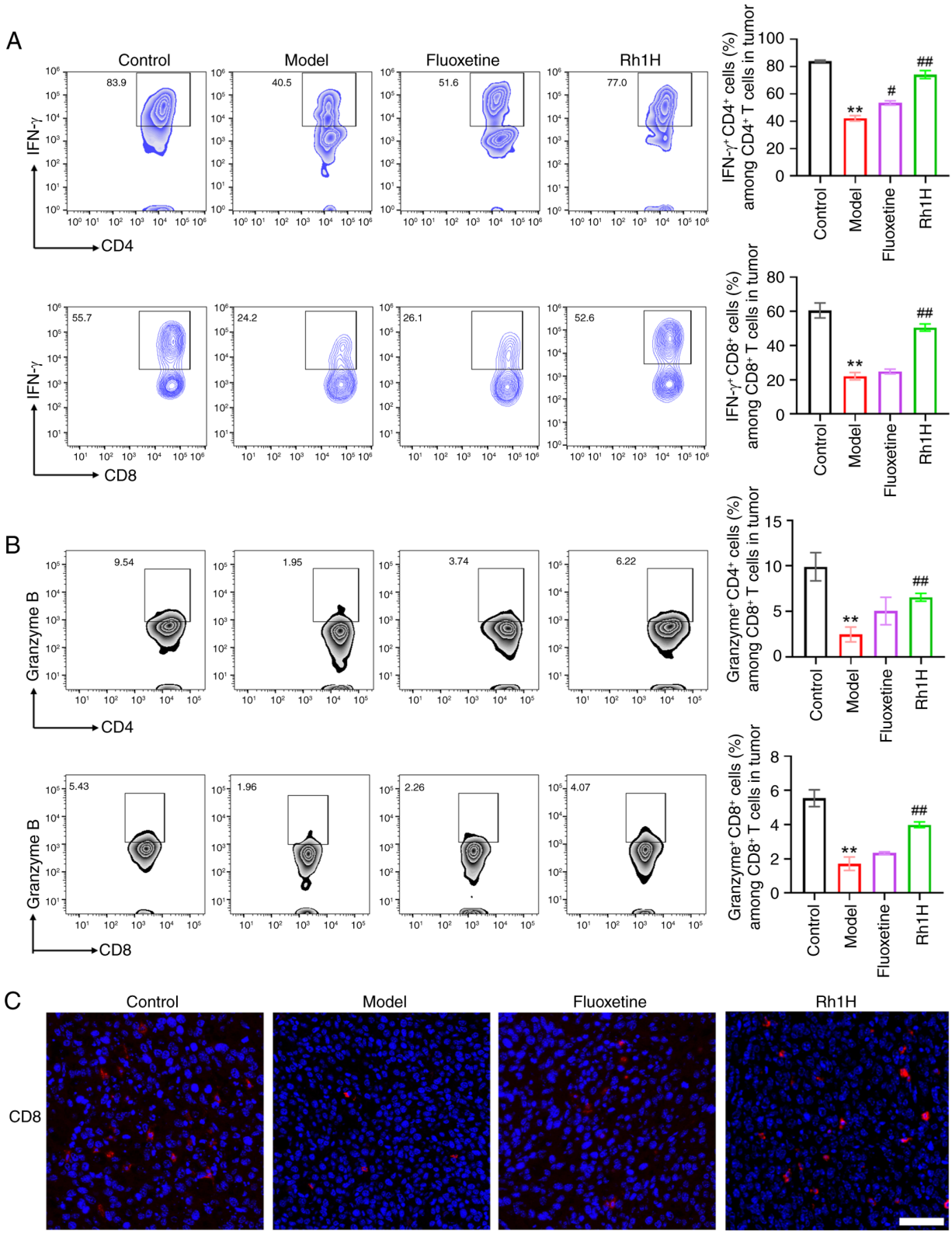

Figure 6. Rh1 promotes the infiltration of T cells into the tumors of mice subjected to chronic restraint stress and bearing colorectal tumors. Intracellular (A) IFN-γ and (B) granzyme B levels in $CD8^+$T and $CD4^+$T cells in colorectal tumors, detected by flow cytometry. n=3. **P<0.01 vs. the control group; $^{\#}$P<0.05 and $^{\#\#}$P<0.01 vs. the model group. (C) Immunofluorescent staining of CD8 expression in the tumor tissue; scale bar, 50 μm. Rh1, ginsenoside Rh1; Rh1H, high dose Rh1.

unclear. Cognitive impairments and depression-like behaviors have been noted in mice subjected to CRS, and ginsenoside Rb1 was shown to prevent these depression-like behaviors (43). Similarly, Rg1 exhibits antidepressant-like effects in rats subjected to CRS (44). Rb1 also significantly attenuated azoxymethane/dextran sodium sulfate-induced colon carcinogenesis in mice (45), while Rg1 demonstrated antitumor activity in a CT26 CRC xenograft mouse model (46). However,

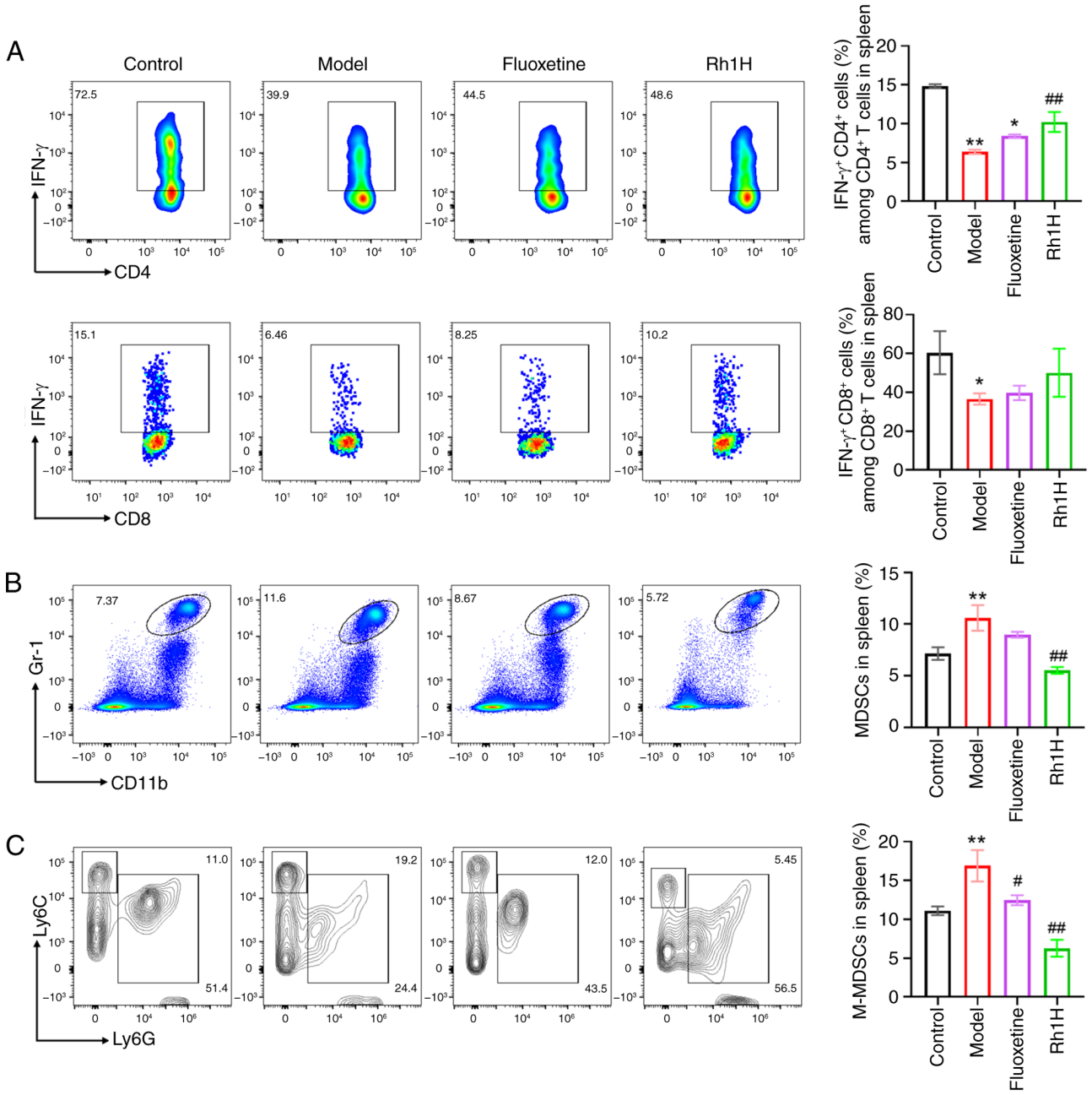

Figure 7. Rh1 treatment promotes T-cell function and reduces the proportion of MDSCs in the spleens of mice subjected to chronic restraint stress and bearing colorectal tumors. (A) Intracellular IFN-γ levels of $CD8^+$T and $CD4^+$T cells in the spleen, analyzed by flow cytometry. (B) MDSC and (C) M-MDSC percentages in the spleen. Representative flow cytometry plots and combined data graphs are shown. n=3. $^*P<0.05$ and $^{**}P<0.01$ vs. the control group; $^{\#}P<0.05$ and $^{\#\#}P<0.01$ vs. the model group. Rh1, ginsenoside Rh1; Rh1H, high dose Rh1; MDSC, myeloid-derived suppressor cell; M-MDSC, monocytic MDSC; Gr-1, granulocyte antigen-1; Ly6C, lymphocyte antigen 6 complex, locus C.

these protective effects of Rb1 or Rg1 were not evaluated in models combining depression with cancer. Therefore, the present study investigated the anticancer and antidepressant potential of Rh1 in CRS-exposed CRC-bearing mice. Previous studies have shown that Rh1 (20 mg/kg) inhibits tumor growth in mice bearing gastric cancer and CRC xenografts (22,47). In addition, fluoxetine (10 mg/kg) was used as a positive control in a previous study on a combined CRS and CRC xenograft model (48). Therefore, it was selected for use as a positive control in the present study. Notably, Rh1 (20 mg/kg) significantly mitigated the depression-like behaviors of mice subjected to CRS in the present study. In addition, the findings of the study indicate that Rh1 prevents CRC tumor growth in mice subjected to CRS.

There is a significant association between depression and the brain-gut axis. Therefore, the preservation and restoration of the normal state of the intestinal flora is considered beneficial for the prevention and treatment of mental disorders (49). In the present study, the results indicated that CRS is positively associated with the progression of CRC, likely by affecting the balance of intestinal flora. Consistent with previous reports, Firmicutes and Bacteroidota were the most common phyla identified across all groups (50). An increased abundance of Firmicutes and a decreased proportion of Bacteroidota were

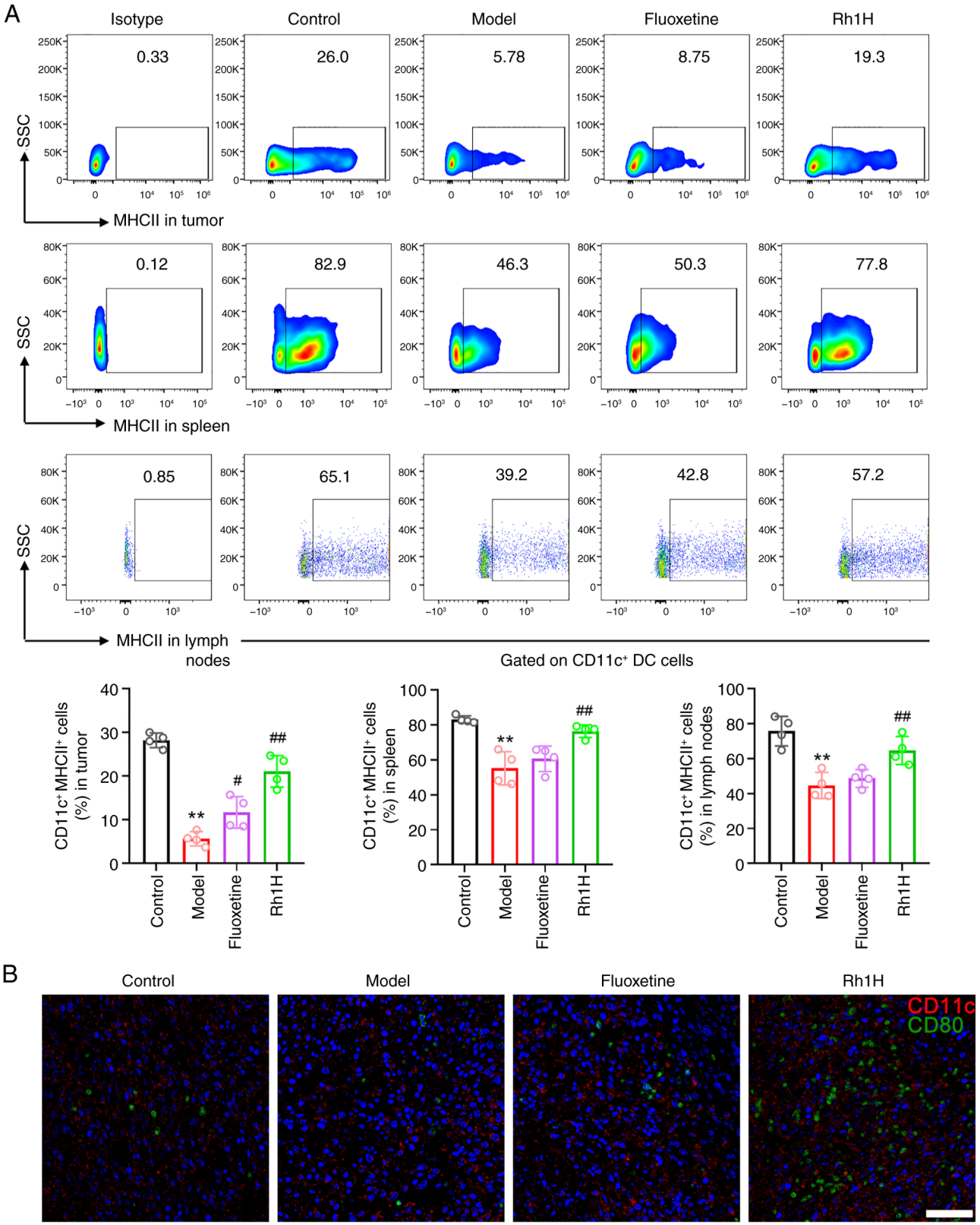

Figure 8. Rh1 treatment promotes DC maturation. (A) Populations of MHCII$^+$CD11c$^+$DCs, considered to represent mature DCs, in the spleen, tumor and tumor-draining lymph nodes of mice bearing colorectal tumors and subjected to chronic restraint stress. (B) Immunofluorescent staining of CD11c (red) and CD80 (green) in the tumors; scale bar, 50 μm. n=3. **P<0.01 vs. the control group; $^{\#}$P<0.05 and $^{\#\#}$P<0.01 vs. the model group. Rh1, ginsenoside Rh1; Rh1H, high dose Rh1; MHCII, major histocompatibility complex class II; DC, dendritic cell; SSC, side scatter.

observed in the CRS-exposed xenografted mice in the present study, which is consistent with previous observations (51). However, treatment with a high dose of Rh1 attenuated these changes, lowering the abundance of Firmicutes and increasing that of Bacteroidota compared with the respective abundances in the CRS model mice.

Due to the complexity of depression, the relationship between the Firmicutes/Bacteriodota ratio and depression remains unclear. However, the oral administration of probiotics or fecal microbiota transplantation (FMT) has been shown to restore the microbial balance of the gut and alleviate dysbiosis (52). For example, the introduction of a probiotic mixture containing six *Bifidobacteria* and *Lactobacillus* strains to patients following CRC surgery lead to a significant reduction in the serum levels of pro-inflammatory cytokines and improved the intestinal microenvironment (53).

The findings of the present study suggest that gut flora at least partially mediate the effects of Rh1 in mice with CRS and CRC, supporting the notion that changes in the gut flora may play a role in the pathophysiology of patients with CRC and comorbid depression. This aligns with clinical evidence that dysregulation of the gut microbiota contributes to CRC development, metastasis and treatment resistance (54). In patients with CRC who have a bacterial infection and require treatment with antibiotics, probiotics supplementation or FMT from a healthy donor may represent a supportive strategy (55). However, future research is necessary to validate these findings and address current limitations.

Immunological dysregulation contributes to the development of depression and can hinder antidepressant treatment outcomes. A study demonstrated that chronic stress increases the proportions of tumor-associated macrophages and MDSCs in the TME, while decreasing the activity of $CD8^+$T cells. In addition, the study revealed that splenic $CD11b^+Gr\text{-}1^{int}Ly6C^{hi}$ myeloid cells induce tolerance in memory $CD8^+$T cells (56). Notably, patients with major depressive disorder exhibit altered numbers of monocytes, $CD4^+$ and $CD8^+$ T cells in the peripheral circulation compared with those in healthy individuals (57). The most potent antigen-presenting cells are DCs, which are crucial components of the adaptive immune response. During maturation, DCs increase the secretion of inflammatory or anti-inflammatory cytokines and upregulate MHCII expression, while mature DCs provide processed antigens to naïve T cells in adjacent lymphatic organs (58). In the present study, a reduction in the quantity of $CD8^+$T and $CD4^+$T cells infiltrating the CRC tissue and producing IFN-γ and granzyme B was observed, which was attenuated by Rh1 treatment. These findings suggest that the functions of DC and T cells were suppressed in CRC tumor-bearing mice subjected to CRS, and that such a repression was mitigated by treatment with Rh1.

Depression and cancer progression have both been associated with MDSC proliferation, which suppresses the immune response (59). Consistent with this, the CRS model mice in the present study displayed a significantly elevated percentage of MDSCs than those in the control group, whereas treatment with Rh1 reduced the frequency of monocytic MDSCs.

Immune dysregulation and heightened inflammatory responses are recognized as contributors to depression, particularly in vulnerable individuals (60). Consistent with this, anti-inflammatory treatments decrease depressive symptoms (61-63). Elevated levels of the proinflammatory cytokines IL-6, IL-1β and TNF-α have been reported in patients with depression (64); therefore, peripheral blood levels of these cytokines have been proposed as indicators of depression (65). In addition, chronically stressed tumor-bearing animals also exhibit elevated levels of TNF-α, IFN-γ and IL-6, which is consistent with the inflammatory hypotheses of depression and may accelerate the development of cancer (66). In the present study, persistent CRS stress increased the release of IL-6, TNF-α and CXCL1 into the serum of tumor-bearing mice, potentially contributing to the progression of CRS. Notably, mice treated with Rh1 had significantly reduced serum levels of these proinflammatory cytokines compared with those in the model group, suggesting that Rh1 exerts anti-inflammatory and antitumor effects under CRS conditions.

The present study has several limitations. Firstly, no electroencephalogram (EEG) activity data were collected to detect if any changes in brain electrical activity associated with depressive symptoms occurred. In future studies, active collaboration with an institution equipped with EEG detection facilities will be sought to investigate the neuroelectrophysiological mechanisms of Rh1, with the aim of obtaining more comprehensive evidence for its therapeutic effects. Second, the 16S rRNA sequencing used to analyze gut microbiota has a relatively low resolution and cannot distinguish closely related species. The results revealed differences in the microbiota of certain groups at the phylum level, as exemplified by the abundances of Proteobacteria, Firmicutes, Bacteriodota and Actinobacteriota. Some data obtained on bacterial genera displayed non-normal distributions and heterogeneous variance. After using appropriate statistical tests, namely Welch's ANOVA or Kruskal-Wallis, non-significant differences in bacterial genera were detected among groups for certain genera, including *Bifidobacterium*, *Romboutsia* and *Alistipes*. In future studies, the sample size will be expanded and metagenomic sequencing performed to explore the effect of Rh1 on microorganisms more deeply. Metagenomic sequencing can also be used to gain whole-genome information and achieve species- or strain-level resolution, with high sensitivity in the identification of low-abundance species.

In conclusion, Rh1 shows promise as an adjunctive therapy for CRC by reducing tumor growth, alleviating depression-like behaviors, and restoring intestinal flora and immunological homeostasis in CRC-xenografted mice under CRS. These findings reveal a novel bioactivity of Rh1 derived from ginseng, which has potential as a novel strategy to improve the outcomes of patients with CRC and associated depressive symptoms. To obtain direct evidence of its interaction with existing therapies, future research should prioritize preclinical trials combining Rh1 with chemotherapy, immunotherapy or targeted agents to evaluate their potential effects on tumor growth and survival.

Acknowledgements

Not applicable.

Funding

This study was supported by the Key Project of TCM Science and Technology Development Plan of Jiangsu Province (grant nos. ZD202415 and ZD202320), Nanjing Medical Institution Traditional Chinese Medicine Preparation Research Project (grant no. NJCC-ZJ-202426), Key Research Project of Jiangsu Provincial Health Commission (grant no. K2023033), Jiangsu Clinical

Innovation Center of Digestive Cancer of Traditional Chinese Medicine (grant no. 2021.6), Jiangsu Provincial Association for Maternal and Child Health Studies (grant no. JSFY202202), Traditional Chinese Medicine Clinical Transformation of Public Service Platform in Jiangsu Province (grant no. BM2023005), Postgraduate Research & Practice Innovation Program of Jiangsu Province (grant no. SJCX24_0881) and Post-subsidy Project for High-Quality Research Achievements of Jiangsu Province Academy of Traditional Chinese Medicine (grant nos. HBZ202501 and HBZ202405).

Availability of data and materials

The high-throughput 16S rRNA sequencing data generated in the present study may be found in the NCBI Sequence Read Archive under the accession number PRJNA1288220 and may be accessed using the following URL: https://www.ncbi.nlm.nih.gov/bioproject/PRJNA1288220. All other data generated in the present study may be requested from the corresponding author.

Authors' contributions

TD, SS and SL conceived and designed the experiments. TD, LL and JS performed the experiments. TD, LL and JL revised the manuscript. JL, TD, XT, XW and YL analyzed and interpreted the data. LL wrote the manuscript. All authors read and approved the final version of the manuscript. TD and SS confirm the authenticity of all the raw data.

Ethics approval and consent to participate

All experimental procedures were authorized by the Institutional Animal Care and Use Committee of Jiangsu Province Academy of Traditional Chinese Medicine (approval nos. AEWC-20230902-327 and AEWC-20240301-391). Jiangsu Province Academy of Traditional Chinese Medicine is an alternative name for Nanjing Integrated Traditional Chinese and Western Medicine Hospital Affiliated with Nanjing University of Chinese Medicine. All animal experiments were performed in compliance with the National Institutes of Health Guide for the Care and Use of Laboratory animals (NIH Publication no. 8023, amended 1978) and described in compliance with the ARRIVE guidelines.

Patient consent for publication

Not applicable.

Competing interests

The authors declare that they have no competing interests.

References

1. Salvucci M, Crawford N, Stott K, Bullman S, Longley DB and Prehn JHM: Patients with mesenchymal tumours and high Fusobacteriales prevalence have worse prognosis in colorectal cancer (CRC). Gut 71: 1600-1612, 2022.
2. Zhao N, Lai C, Wang Y, Dai S and Gu H: Understanding the role of DNA methylation in colorectal cancer: Mechanisms, detection, and clinical significance. Biochim Biophys Acta Rev Cancer 1879: 189096, 2024.
3. Zheng Z, Hou X, Bian Z, Jia W and Zhao L: Gut microbiota and colorectal cancer metastasis. Cancer Lett 555: 216039, 2023.
4. Wang J and Liao ZX: Research progress of microrobots in tumor drug delivery. Food Med Homol 1: 9420025, 2024.
5. Ye L, Hou Y, Hu W, Wang H, Yang R, Zhang Q, Feng Q, Zheng X, Yao G and Hao H: Repressed Blautia-acetate immunological axis underlies breast cancer progression promoted by chronic stress. Nat Commun 14: 6160, 2023.
6. Yang S, Li Y, Zhang Y and Wang Y: Impact of chronic stress on intestinal mucosal immunity in colorectal cancer progression. Cytokine Growth Factor Rev 80: 24-36, 2024.
7. Otun S, Achilonu I and Odero-Marah V: Unveiling the potential of Muscadine grape Skin extract as an innovative therapeutic intervention in cancer treatment. J Funct Foods 116: 106146, 2024.
8. Urakami H, Yoshikawa S, Nagao K, Miyake K, Fujita Y, Komura A, Nakashima M, Umene R, Sano S, Hu Z, *et al*: Stress-experienced monocytes/macrophages lose anti-inflammatory function via β2-adrenergic receptor in skin allergic inflammation. J Allergy Clin Immunol 155: 865-879, 2025.
9. Globig AM, Zhao S, Roginsky J, Maltez VI, Guiza J, Avina-Ochoa N, Heeg M, Araujo Hoffmann F, Chaudhary O, Wang J, *et al*: The β1-adrenergic receptor links sympathetic nerves to T cell exhaustion. Nature 622: 383-392, 2023.
10. Zhang S, Yu F, Che A, Tan B, Huang C, Chen Y, Liu X, Huang Q, Zhang W, Ma C, *et al*: Neuroendocrine regulation of stress-induced T cell dysfunction during lung cancer immunosurveillance via the kisspeptin/GPR54 signaling pathway. Adv Sci (Weinh) 9: e2104132, 2022.
11. Wang XH, Fu YL, Xu YN, Zhang PC, Zheng TX, Ling CQ and Feng YL: Ginsenoside Rh1 regulates the immune microenvironment of hepatocellular carcinoma via the glucocorticoid receptor. J Integr Med 22: 709-718, 2024.
12. Sommershof A, Scheuermann L, Koerner J and Groettrup M: Chronic stress suppresses anti-tumor T(CD8+) responses and tumor regression following cancer immunotherapy in a mouse model of melanoma. Brain Behav Immun 65: 140-149, 2017.
13. Zhou M, Fan Y, Xu L, Yu Z, Wang S, Xu H, Zhang J, Zhang L, Liu W, Wu L, *et al*: Microbiome and tryptophan metabolomics analysis in adolescent depression: Roles of the gut microbiota in the regulation of tryptophan-derived neurotransmitters and behaviors in human and mice. Microbiome 11: 145, 2023.
14. Zou Y, Wang S, Zhang H, Gu Y, Chen H, Huang Z, Yang F, Li W, Chen C, Men L, *et al*: The triangular relationship between traditional Chinese medicines, intestinal flora, and colorectal cancer. Med Res Rev 44: 539-567, 2024.
15. Zheng W, Shen P, Yu C, Tang Y, Qian C, Yang C, Gao M, Wu Y, Yu S, Tang W, *et al*: Ginsenoside Rh1, a novel casein kinase II subunit alpha (CK2α) inhibitor, retards metastasis via disrupting HHEX/CCL20 signaling cascade involved in tumor cell extravasation across endothelial barrier. Pharmacol Res 198: 106986, 2023.
16. Hou J, Xue J, Lee M, Yu J and Sung C: Long-term administration of ginsenoside Rh1 enhances learning and memory by promoting cell survival in the mouse hippocampus. Int J Mol Med 33: 234-240, 2014.
17. Zhang L, Gao X, Yang C, Liang Z, Guan D, Yuan T, Qi W, Zhao D, Li X, Dong H and Zhang H: Structural characters and pharmacological activity of protopanaxadiol-type saponins and protopanaxatriol-type saponins from ginseng. Adv Pharmacol Pharm Sci 2024: 9096774, 2024.
18. Wang H, Yang Y, Yang S, Ren S, Feng J, Liu Y, Chen H and Chen N: Ginsenoside Rg1 ameliorates neuroinflammation via suppression of connexin43 ubiquitination to attenuate depression. Front Pharmacol 12: 709019, 2021.
19. Han D, Zhao Z, Mao T, Gao M, Yang X and Gao Y: Ginsenoside Rg1: A neuroprotective natural dammarane-type triterpenoid saponin with anti-depressive properties. CNS Neurosci Ther 30: e70150, 2024.
20. Wang YZ, Chen J, Chu SF, Wang YS, Wang XY, Chen NH and Zhang JT: Improvement of memory in mice and increase of hippocampal excitability in rats by ginsenoside Rg1's metabolites ginsenoside Rh1 and protopanaxatriol. J Pharmacol Sci 109: 504-510, 2009.
21. Nahar J, Boopathi V, Murugesan M, Rupa EJ, Yang DC, Kang SC and Mathiyalagan R: Investigating the anticancer activity of G-Rh1 using in silico and in vitro studies (A549 Lung Cancer Cells). Molecules 27: 8311, 2022.
22. Lyu X, Xu X, Song A, Guo J, Zhang Y and Zhang Y: Ginsenoside Rh1 inhibits colorectal cancer cell migration and invasion in vitro and tumor growth in vivo. Oncol Lett 18: 4160-4166, 2019.

23. Jin Y, Huynh DTN and Heo KS: Ginsenoside Rh1 inhibits tumor growth in MDA-MB-231 breast cancer cells via mitochondrial ROS and ER stress-mediated signaling pathway. Arch Pharm Res 45: 174-184, 2022.
24. Jiang Y, Hu Y, Yang Y, Yan R, Zheng L, Fu X, Xiao C and You F: Tong-Xie-Yao-Fang promotes dendritic cells maturation and retards tumor growth in colorectal cancer mice with chronic restraint stress. J Ethnopharmacol 319 (Pt 1): 117069, 2024.
25. Olescowicz G, Neis VB, Fraga DB, Rosa PB, Azevedo DP, Melleu FF, Brocardo PS, Gil-Mohapel J and Rodrigues ALS: Antidepressant and pro-neurogenic effects of agmatine in a mouse model of stress induced by chronic exposure to corticosterone. Prog Neuropsychopharmacol Biol Psychiatry 81: 395-407, 2018.
26. Wang W, Liu L, Yang X, Gao H, Tang QK, Yin LY, Yin XY, Hao JR, Geng DQ and Gao C: Ketamine improved depressive-like behaviors via hippocampal glucocorticoid receptor in chronic stress induced-susceptible mice. Behav Brain Res 364: 75-84, 2019.
27. Wu X, Shetty AK and Reddy DS: Long-term changes in neuroimaging markers, cognitive function and psychiatric symptoms in an experimental model of Gulf War Illness. Life Sci 285: 119971, 2021.
28. Liu L, Liu Y, Li R, Teng Y, Zhao S, Chen J, Li C, Hu X and Sun L: Identification of critical signature in post-traumatic stress disorder using bioinformatics analysis and in vitro analyses. Brain Behav 15: e70243, 2025.
29. Wu J, Zhang T, Yu L, Huang S, Yang Y, Yu S, Li J, Cao Y, Wei Z, Li X, *et al*: Zhile capsule exerts antidepressant-like effects through upregulation of the BDNF signaling pathway and neuroprotection. Int J Mol Sci 20: 195, 2019.
30. Sui H, Zhang L, Gu K, Chai N, Ji Q, Zhou L, Wang Y, Ren J, Yang L, Zhang B, *et al*: YYFZBJS ameliorates colorectal cancer progression in Apc(Min/+) mice by remodeling gut microbiota and inhibiting regulatory T-cell generation. Cell Commun Signal 18: 113, 2020.
31. Simpson EH: Measurement of diversity. Nature 163: 688, 1949.
32. Chao A and Lee SM: Estimating the number of classes via sample coverage. J Am Stat Assoc 87: 210-217, 1992.
33. Shannon CE: Shannon CE. A mathematical theory of communication. Bell System Technical Journal 27: 379-423, 1948
34. Ren Q, He C, Sun Y, Gao X, Zhou Y, Qin T, Zhang Z, Wang X, Wang J, Wei S and Wang F: Asiaticoside improves depressive-like behavior in mice with chronic unpredictable mild stress through modulation of the gut microbiota. Front Pharmacol 15: 1461873, 2024.
35. Zhao L, Zhu X, Ni Y, You J and Li A: Xiaoyaosan, a traditional Chinese medicine, inhibits the chronic restraint stress-induced liver metastasis of colon cancer in vivo. Pharm Biol 58: 1085-1091, 2020.
36. Yan X, Shi L, Zhu X, Zhao Y, Luo J, Li Q, Xu Z and Zhao J: From microbial homeostasis to systemic pathogenesis: A narrative review on gut flora's role in neuropsychiatric, metabolic, and cancer disorders. J Inflamm Res 18: 8851-8873, 2025.
37. Chu Y, Qian L, Ke Y, Feng X, Chen X, Liu F, Yu L, Zhang L, Tao Y, Xu R, *et al*: Lymph node-targeted neoantigen nanovaccines potentiate anti-tumor immune responses of post-surgical melanoma. J Nanobiotechnology 20: 190, 2022.
38. Hao Y, Ge H, Sun M and Gao Y: Selecting an appropriate animal model of depression. Int J Mol Sci 20: 4827, 2019.
39. Ding H, Lin J, Xu Z, Wang HHX, Huang L, Huang J and Wong MCS: The association between organised colorectal cancer screening strategies and reduction of its related mortality: A systematic review and meta-analysis. BMC Cancer 24: 365, 2024.
40. He L, Tian Y, Liu Q, Bao J and Ding RB: Antidepressant sertraline synergistically enhances paclitaxel efficacy by inducing autophagy in colorectal cancer cells. Molecules 29: 3733, 2024.
41. Huynh DTN, Jin Y, Myung CS and Heo KS: Ginsenoside Rh1 induces MCF-7 cell apoptosis and autophagic cell death through ROS-Mediated Akt signaling. Cancers (Basel) 13: 1892, 2021.
42. Mathiyalagan R, Wang C, Kim YJ, Castro-Aceituno V, Ahn S, Subramaniyam S, Simu SY, Jiménez-Pérez ZE, Yang DC and Jung SK: Preparation of polyethylene glycol-ginsenoside Rh1 and Rh2 conjugates and their efficacy against lung cancer and inflammation. Molecules 24: 4367, 2019.
43. Guo Y, Xie J, Zhang L, Yang L, Ma J, Bai Y, Ma W, Wang L, Yu H, Zeng Y, *et al*: Ginsenoside Rb1 exerts antidepressant-like effects via suppression inflammation and activation of AKT pathway. Neurosci Lett 744: 135561, 2021.
44. Li J, Gao W, Zhao Z, Li Y, Yang L, Wei W, Ren F, Li Y, Yu Y, Duan W, *et al*: Ginsenoside Rg1 reduced microglial activation and mitochondrial dysfunction to alleviate depression-like behaviour via the GAS5/EZH2/SOCS3/NRF2 axis. Mol Neurobiol 59: 2855-2873, 2022.
45. Wang L, Zhang QQ, Xu YY, Zhang R, Zhao Q, Zhang YQ, Huang XH, Jiang B and Ni M: Ginsenoside Rb1 Suppresses AOM/DSS-induced colon carcinogenesis. Anticancer Agents Med Chem 23: 1067-1073, 2023.
46. Liu R, Zhang B, Zou S, Cui L, Lin L and Li L: Ginsenoside Rg1 induces autophagy in colorectal cancer through inhibition of the Akt/mTOR/p70S6K pathway. J Microbiol Biotechnol 34: 774-782, 2024.
47. Yang Z, Wu X, Shen J, Gudamu A, Ma Y, Zhang Z and Hou M: Ginsenoside Rh1 regulates gastric cancer cell biological behaviours and transplanted tumour growth in nude mice via the TGF-β/Smad pathway. Clin Exp Pharmacol Physiol 49: 1270-1280, 2022.
48. Zhang Z, Shao S, Zhang Y, Jia R, Hu X, Liu H, Sun M, Zhang B, Li Q and Wang Y: Xiaoyaosan slows cancer progression and ameliorates gut dysbiosis in mice with chronic restraint stress and colorectal cancer xenografts. Biomed Pharmacother 132: 110916, 2020.
49. Gao Y: Inflammation and gut microbiota in the alcoholic liver disease. Food Med Homol 1: 9420020, 2024.
50. Wang J, Fan L, Teng T, Wu H, Liu X, Yin B, Li X, Jiang Y, Zhao J, Wu Q, *et al*: Adolescent male rats show altered gut microbiota composition associated with depressive-like behavior after chronic unpredictable mild stress: Differences from adult rats. J Psychiatr Res 173: 183-191, 2024.
51. Shao S, Jia R, Zhao L, Zhang Y, Guan Y, Wen H, Liu J, Zhao Y, Feng Y, Zhang Z, *et al*: Xiao-Chai-Hu-Tang ameliorates tumor growth in cancer comorbid depressive symptoms via modulating gut microbiota-mediated TLR4/MyD88/NF-κB signaling pathway. Phytomedicine 88: 153606, 2021.
52. Xu JY, Liu MT, Tao T, Zhu X and Fei FQ: The role of gut microbiota in tumorigenesis and treatment. Biomed Pharmacother 138: 111444, 2021.
53. Zaharuddin L, Mokhtar NM, Muhammad Nawawi KN and Raja Ali RA: A randomized double-blind placebo-controlled trial of probiotics in post-surgical colorectal cancer. BMC Gastroenterol 19: 131, 2019.
54. Piccinno G, Thompson KN, Manghi P, Ghazi AR, Thomas AM, Blanco-Míguez A, Asnicar F, Mladenovic K, Pinto F, Armanini F, *et al*: Pooled analysis of 3,741 stool metagenomes from 18 cohorts for cross-stage and strain-level reproducible microbial biomarkers of colorectal cancer. Nat Med 31: 2416-2429, 2025.
55. Jamal R, Messaoudene M, de Figueiredo M and Routy B: Future indications and clinical management for fecal microbiota transplantation (FMT) in immuno-oncology. Semin Immunol 67: 101754, 2023.
56. Ugel S, Peranzoni E, Desantis G, Chioda M, Walter S, Weinschenk T, Ochando JC, Cabrelle A, Mandruzzato S and Bronte V: Immune tolerance to tumor antigens occurs in a specialized environment of the spleen. Cell Rep 2: 628-639, 2012.
57. Foley ÉM, Parkinson JT, Mitchell RE, Turner L and Khandaker GM: Peripheral blood cellular immunophenotype in depression: A systematic review and meta-analysis. Mol Psychiatry 28: 1004-1019, 2023.
58. Shi H, He J, Li X, Han J, Wu R, Wang D, Yang F and Sun E: Isorhamnetin, the active constituent of a Chinese herb Hippophae rhamnoides L, is a potent suppressor of dendritic-cell maturation and trafficking. Int Immunopharmacol 55: 216-222, 2018.
59. Lu YT, Li J, Qi X, Pei YX, Shi WG and Lin HS: Effects of Shugan Jianpi Formula () on myeloid-derived suppression cells-mediated depression breast cancer mice. Chin J Integr Med 23: 453-460, 2017.
60. Bai Y, Cai Y, Chang D, Li D, Huo X and Zhu T: Immunotherapy for depression: Recent insights and future targets. Pharmacol Ther 257: 108624, 2024.
61. Du Y, Dou Y, Wang M, Wang Y, Yan Y, Fan H, Fan N, Yang X and Ma X: Efficacy and acceptability of anti-inflammatory agents in major depressive disorder: A systematic review and meta-analysis. Front Psychiatry 15: 1407529, 2024.
62. Baghdadi LR: Tocilizumab reduces depression risk in rheumatoid arthritis patients: A systematic review and meta-analysis. Psychol Res Behav Manag 17: 3419-3441, 2024.

63. Iyengar RL, Gandhi S, Aneja A, Thorpe K, Razzouk L, Greenberg J, Mosovich S and Farkouh ME: NSAIDs are associated with lower depression scores in patients with osteoarthritis. Am J Med 126: 1017.e11-8, 2013.
64. Drago A, Crisafulli C, Calabrò M and Serretti A: Enrichment pathway analysis. The inflammatory genetic background in Bipolar Disorder. J Affect Disord 179: 88-94, 2015.
65. Argue BMR, Casten LG, McCool S, Alrfooh A, Richards JG, Wemmie JA, Magnotta VA, Williams AJ, Michaelson J, Fiedorowicz JG, *et al*: Immune dysregulation in bipolar disorder. J Affect Disord 374: 587-597, 2025.
66. Dai S, Mo Y, Wang Y, Xiang B, Liao Q, Zhou M, Li X, Li Y, Xiong W, Li G, *et al*: Chronic stress promotes cancer development. Front Oncol 10: 1492, 2020.